Progress in Oceanography 216 (2023) 103057

Contents lists available at ScienceDirect

Progress in Oceanography

journal homepage: www.elsevier.com/locate/pocean

A case study off the Tiwi Islands and the Coburg Peninsula: Baroclinic on one side and barotropic on the other

R. Robertson [a,*], C. Zhao [b], W. Wang [b], Z. Xu [b], Z. Liu [c]

[a] China-Asean College of Marine Science, Xiamen University Malaysia, Sepang, Malaysia
[b] CAS Key Laboratory of Ocean Circulation and Waves, Institute of Oceanology, Chinese Academy of Sciences Qingdao, China
[c] State Key Laboratory of Marine Environmental Science, and Department of Physical Oceanography, College of Ocean and Earth Sciences, Xiamen University, Xiamen, China

A B S T R A C T

Observational data (ADCP and CTD) were collected from two areas on either side of the Tiwi Islands and Coburg Peninsula. Tides dominated the ocean dynamics in both areas, with contributions from solar radiation, nighttime convective cooling, surface wind mixing, and benthic frictional mixing. Despite the same dominating forcing factors, the dynamics and envrionments differed between the east and west sides of the Tiwi Islands and Coburg Peninsula. The east side was baroclinic with internal tides present along with tidal advection; however, the west side was barotropic and dominated by tidal advection of warmer, saltier water from shallower areas past the observation site with essentially no internal tides. The daily solar radiation cycle's influence reached the bottom on the western side, but was limited to above the thermocline on the eastern side. There, fluorescence was limited to the lower layer, whereas on the western side, it encompassed the entire water column in daytime and peaked below the upper layer, where warmer and higher oxygenated water were generated by solar radiation and surface mixing. Fluorescence vertically integrated over the water column was much higher on the eastern side than the western side. Fluorescence peaks also differed temporally between the east and west sides, with the eastern side dominated by semidiurnal tides and the western side by the daily solar cycle. These dynamics have distinct implications for biological activity and primary productivity.

1. Introduction

Near the Tiwi Islands and Coburg Peninsula, both observational and simulated oceanographic data are sparse, resulting in very little information for the region. There have been very few physical oceanographic studies of the Timor and Arafura seas. Furthermore, most of the investigations were modelling studies that covered a broad area [Schiller, 2011] or focused either on the Gulf of Carpentaria [Condie, 2011] or on the northern region [Kampf, 2016]. *Kampf* [2015] used a model to investigate plankton blooms due to upwelling in the Arafura Sea. He found little response near the Tiwi Islands; however, a strong response in the northwest Arafura Sea, suggesting a lack of upwelling near the Tiwi Islands. Using a model, *Condie* [2011] determined the general flow was northeast off Melville Island, the largest of the Tiwi Islands and was not wind-driven, but rather triggered by the general circulation. He found he long-term transports in the Timor Sea were dominated by the seasonal monsoons and associated winds [Condie, 2011]. Strong alongshore or on-offshore currents are not present near the islands. *Condie* [2011] also indicated that wind-induced upwelling of nutrient-rich deeper waters and other mixing mechanisms are important factors for biological productivity in these oligotrophic waters. However, upwelling occurs further offshore than the Tiwi Islands, closer to deep water. All three of the modeling studies point out that tides are a major factor for the region near the Tiwi Islands and Coburg Peninsula. Like the modeling studies, there is a paucity of observational data for the region, which could be used for understaning the dynamics and environment of the region and for model validation. Only one observational study [Moore et al., 2019] collected primarily chemical and biological observations in the area, using water samples. There are several moorings north of this region as part of the Integrated Marine Observing System (IMOS https://imos.org.au/), but most of them are much further offshore, and experience different dynamics. Two moorings are relatively near our observation sites: DAR and LYN (Fig. 1). Physical oceanographic information on the circulation and mixing is important for resupply of nutrients, biological productivity, and initialization and verification of regional models and would be useful for a proposed tidal power station site [*Tenex* Energy, 2019]. In summary, there is very little information on the dynamics and mixing in this region in either observations or simulations.

The dynamics and environment of a location are typically controlled by the forces involved. Generally, the primary processes involved in ocean dynamics are: major geostrophic currents, longshore coastal

* Corresponding author.
E-mail address: robin.robertson@xmu.edu.my (R. Robertson).

https://doi.org/10.1016/j.pocean.2023.103057
Received 7 March 2023; Received in revised form 30 May 2023; Accepted 5 June 2023
Available online 9 June 2023

currents, wind, tides, eddies, upwelling, and the daily solar radiation cycle. However, in the southern Timor and Arafura seas near the Tiwi Islands, Coburg Peninsula, and Darwin (Fig. 1), there are no major geostrophic currents, strong coastal currents, or eddies [Condie, 2011; Schiller, 2011; Kampf, 2016]. A weak coastal current does flow north from the Gulf of Carpenteria on the east side of Coburg Peninsula and then west north of the Tiwi Islands, but the flow is weak in the shallow waters near the islands and stronger further offshore [Condie, 2011]. However, the tides there are quite large [Easton, 1970] with a maximum range of ~ 8 m at Darwin [https://www.darwinport.com.au/safety-environment/environment; Chapman, 1903]. The daily solar cycle is strong, due to its location at 11-12°S. Its tropical location, a little south of the doldrums and Intertropical Convergence Zone (ITZC), results in typically weak winds, although daily sea breezes and thunderstorms are common. The generally sluggish winds along with a low Coriolis parameter, inhibit upwelling events. Consequently, the potential forces for the circulation and mixing are limited primarily to tides and the daily solar radiation/nighttime cooling cycle, with daily sea breezes and benthic friction contributing in minor ways, primarily through mixing.

The primary forcing for this region is the strong tides, which have several roles in ocean dynamics in shallow water: 1) they advect water on– and off-shore.; 2) they generate tidal fronts by mixing the entire water column; 3) baroclinic tides induce mixing through shear instabilities; 4) they affect the available light for photosynthesis by shifting the depth of the thermocline [Stevens et al., 2012]; 5) they alternately entrain and deposit both phytoplankton and sediment through the alternating strength of the tidal velocities [Cloern et al., 1991; Blauw et al., 2012]; 6) tidal currents induce benthic mixing through frictional stress against the bottom [Robertson 2006; Robertson and Dong, 2019]; 7) they also advect biological species back and forth during the ebb and flood tidal cycle [Cloern et al., 1991; Sharples et al., 2007; Blauw et al., 2012]. Tides have been found to influence biological productivity and composition in other regions, such as San Francisco Bay [Cloern, 1991] and the North Sea [Blauw et al., 2012], where strong tidal signals were present in biological productivity and species diversity [Cloern, 1991; Blauw et al., 2012]. The predominant mechanisms were: 1) entrainment and sinking due to changes in the magnitude of the tidal currents (period of 6.2 h), 2) advection of different waters during the tidal cycle (period of 12.4 h), and 3) the diurnal cycle (period of 24 h).

Originally, a proposal was granted by Australia's Marine National Facility (MNF) for a voyage on the RV Investigator, IN2019v06 (6th voyage of RV Investigator in 2019), with a combination of atmospheric scientists and oceanographers to study the Indonesian seas. The original overarching goal was to study the transfer of heat and fresh water between the atmosphere and the ocean, including the upper water column. Unfortunately, permission to operate in Indonesia waters was not obtained, so instead the voyage was split into two legs, both in Australian waters. Leg 1 focused on oceanography off Australia's Northwest Shelf in the Timor Sea, but included atmospheric scientists, and Leg 2 on atmospheric science in the Arafura Sea, including physical oceanographers. Since the location changed, the goal also was modified to two goals: to investigate 1) wind and tidal mixing on Leg 1 and 2) Tropical Storm Hector on Leg 2 On both legs, we were still looking at the transfer of heat and fresh water from the atmosphere into the water column. The physical oceanographic conditions during Leg 2 are the focus of this paper. On Leg 2, a variety of underway and profiling instruments were utilized at several sites near the Tiwi Islands and Coburg Peninsula, including collecting several temperature, salinity, and velocity profile time series over roughly 2 day periods. Since the driving forces (strong tides and the daily solar cycle) were essentially the same in both regions,

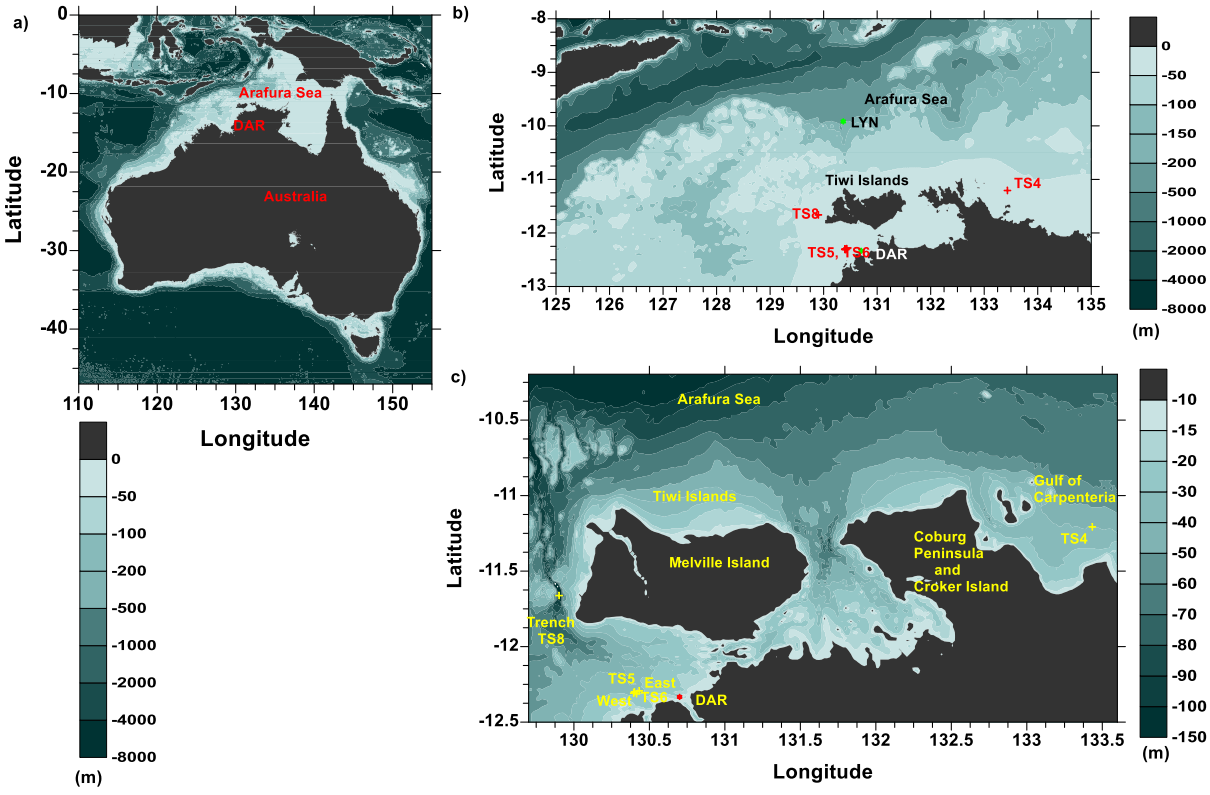

Fig. 1. A) An overview of Australia and the Tiwi Islands based on ETOPO1 bathymetry b) An overview of the Tiwi Islands, Coburg peninsula, and Darwin region with the IMOS LYN mooring location at Lynedoch Backspace Shoals noted by LYN. The bathymetry is ETOPO1, which does not resolve the trench. c) The bathymetry of the Timor and Arafura seas around the Tiwi Islands with the time series locations marked by red crosses and labeled TS4, TS5, and TS6, respectively. The domain used for the model simulation is shown in c). It has been smoothed more than in b). The locations of the casts on the east and west sides of time series 4 and 5 and the casts in the trench (TS8) are also indicated by yellow crosses and labeled. the red dot labeled DAR indicates the location of the IMOS Darwin mooring. The LY mooring location is north of the area shown in c).

we expected conditions to be similar. However, mixing on the west side of the Tiwi Islands and Coburg Peninsula was much stronger, resulting in a barotropic water column with little productivity; whereas, on the east side the water column was baroclinic with two primary layers and high productivity in the lower layer. Our observational program is described in Section 2 and a supporting modeling effort in Section 3. Section 4 gives our results outlining the different conditions and dynamics on the east and west sides of the Tiwi Islands and Coburg Peninsula. Finally, a summary is provided in Section 5.

2. Observational effort

Several times series of hydrographic and velocity profile data were collected from the RV Investigator in the southern Timor and Arafura seas near the Tiwi Islands and Coburg Peninsula off northern Australia between November 12 and December 16, 2019 (Fig. 1 and Table 1). Multiple systems were used to collect the data, including a Conductivity, Temperature, Depth (CTD) profiler measuring pressure, temperature, salinity, dissolved oxygen, fluorescence, and turbidity, a shipboard Acoustic Doppler Current Profiler (SADCP) measuring velocities, and the ship's Underway system measuring a suite of parameters at a depth of ~ 5 m. The time series were roughly two-days long with a CTD cast performed every half hour (Table 1). The first, Time Series 4 (TS4), lasted 51 h and was on the east side of the Tiwi Islands and Coburg Peninsula (Fig. 1). The second and third, Time Series 5 and 6 (TS5 and TS6), lasted 45 and 49 h, respectively, and were on the west side of the Tiwi Islands and Coburg Peninsula (Fig. 1). TS5 was interrupted due to mechanical issues. Time Series 8 (TS8) was on the western side in a trench off the westernmost Tiwi Island (Fig. 1c), but only lasted 9 h. TS4 and TS5/6 are roughly 300 km apart and the width of the Tiwi Islands is roughly 170 km between the easternmost and westernmost extents.

2.1. CTD

Hydrographic profiles were collected using a Sea-Bird SBE911 + CTD attached to a 24-bottle Rosette system. Dual pumps, temperature, conductivity, and oxygen sensors and single transmissometer, nephelometer, Wetlabs ECO-chlorophyll, Wetlabs ECO-scattering, PAR, and altimeter sensors were installed on the CTD. Data was processed using the CSIRO Cappro software version 2.9 and binned at 1 dbar intervals. Temperature and salinity uncertainties were ± 0.0015 °C and ± 0.005 psu, respectively.

2.2. Shipboard ADCP (SADCP)

The SADCP provided velocities over most of the water column in these shallow waters, depths < 50 m, so a Lowered ADCP (LADCP) was not used. A RDI 150 kHz ADCP's was operated nearly continuously from the RV Investigator in broadband mode. It was set with 2 m bins and output data at ~ 5 min intervals, with the exception of the first 2 days when the bin size was 4 m. As the SADCP was mounted on the drop keel, which was at ~ 6.5 m depth, there is no valid velocity data less than ~ 10 m depth. Observational uncertainties were 1–2 cm s^{-1} [Thurnherr, 2010]. Pressure, potential temperature, and density were calculated using the TEOS-10 Matlab routines [https://www.teos-10.org/].

Table 1
The date, time, latitude, longitude, duration, and water depth for each of the Time Series during Leg 2 of IN2019v06. Since two casts were performed per hour, the number of casts is twice the duration in hours plus 1.

Site	Date (UTC 2019)	Start Time (UTC)	Duration (hours)	Latitude (° S)	Longitude (° E)	Water Depth (m)
TS4	14–16 Nov	19:30	51	11°12.4′	133°26.1′	42
TS5	22–24 Nov	19:30	43 + 2	12°18.71′	130°24.1′	29
TS6	3–5 Dec	20:00	49	12°19.2′	130o24.8′	29
TS8	12–13 Dec	15:30	9	11°39.7′	130°43.1	~150

2.3. Underway observations

A wide variety of meteorological and surface ocean data were collected by RV Investigator's underway data system, including wind speed and direction, rain, humidity (Fig. 2), air temperature, sea surface temperature, salinity, dissolved oxygen, fluorescence, turbidity, etc. These were output at 5 s intervals. During this leg of the voyage, the ocean surface data came in from ~ 6.9 m below the surface.

3. Modeling support

To aid in understanding the circulation and tides in the region, simulations were performed for the region using the Regional Ocean Modeling System (ROMS) version 3.4. ROMS is a primitive-equation, sigma-coordinate model [Shchepetkin and McWilliams, 2004], which is widely used for tidal simulations. The tidal simulation was performed on the domain in Fig. 1c with a resolution of ~ 2 km and 25 vertical levels. These simulations were run for 20 days. Bathymetry was obtained from Geoscience Australia [Whiteway, 2009]. The observed hydrography was used as much as possible for initialization of the temperature and salinity in these simulations with additional values as needed from the World Ocean Atlas [Locarnini et al., 2013] for nearby areas without observational data from this voyage. Tidal forcing used eight constituents, M_2, S_2, N_2, K_2, K_1, O_1, P_1, and Q_1, with the coefficients taken from TPXO8.2 [Egbert and Erofeeva, 2002]. These were applied to the 2-D mode elevations and velocities and updated on the 2-D time steps by *Robertson* in 2001. This was done for accuracy and to avoid resonance, particularly near the tidal critical latitudes; however, this technique has not been adopted by the ROMS model in general [2001]. Winds were not included in the tidal simulation for two reasons: 1) the resolution of the available winds were insufficient over the entire region and 2) winds have been found to overmix the upper water column in ROMS [Robertson and Hartlipp, 2017]. The daily solar forcing was included in all simulations using observed values from the ship's underway data (Fig. 2b, 2d, and 2f) and was applied only at the surface. The *Large-McWilliams-Doney/Kpp* (LMD/KPP) vertical mixing parameterization was used.

4. Results and discussion

4.1. Hydrographic conditions

4.1.1. At the time series sites

The hydrographic conditions differed between the east and west sides of the Tiwi Islands and Coburg Peninsula. The time series from the eastern side (TS4) was cooler, fresher, and higher in oxygen (Fig. 3) than the time series on the western side (TS5 and TS6) (Figs. 4 and 5). It should be noted that value ranges for the different potential temperature and salinity in Figs. 3-5 vary between the east and west sides with 28–32.2 °C and 34.20–34.45 psu on the east side and 31.0–32.1 °C and 35.10–35.60 psu on the west side. A clear two layer structure with a thermocline and peak Brunt-Väisälä frequency, > 10 cph. at ~ 20 m was present on the eastern side (Figs. 3 and 6c); however, temperatures and salinities on the western side were nearly uniform with depth (Fig. 4a and 5a) and the highest temperatures and Brunt-Väisälä frequency values were associated with the daily warming and nighttime cooling cycle (Fig. 7c and Fig. 8c).

Temperature fluctuations were largest at the surface and thermocline, ~20 m, on the east side and at the surface on the west side (not shown). The surface fluctuations are attributed to the diurnal cycle. The warm temperature from daytime solar radiation were mixed into the

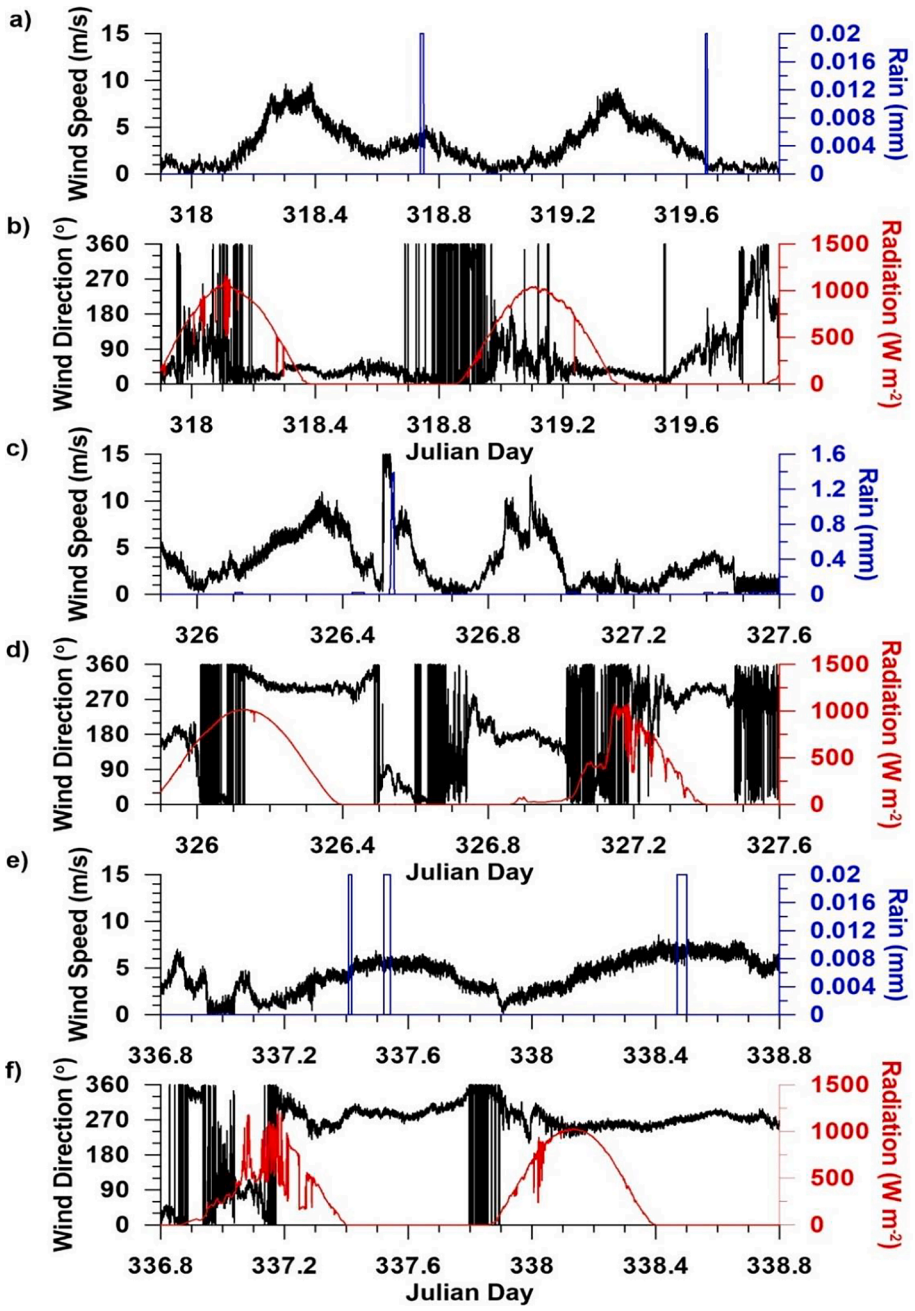

Fig. 2. Wind speed (black) and rain (blue) during Time Series a) 4, c) 5, and e) 6. Wind direction (black) and radiation (red) during Time Series b) 4, d) 5, and f) 6.

upper water column by the afternoon sea breezes (Figs. 3-5). The sea breezes induced waves, which are believed to have both increased the dissolved oxygen content near the surface and mixed the warmer, higher dissolved oxygen water deeper into the water column. This is clearly seen in the potential temperatures, densities, and dissolved oxygen (Fig. 3a, 3c, and 3d, 4a, 4c, and 4d, and 5a, 5c, and 5d for TS4, TS5, and TS6, respectively). It is also apparent as high Brunt-Väisäla frequency values at the corresponding times and depths (Fig. 6c, 7c, and 8c).

4.1.2. The surrounding region

The underway data show warmer temperatures on the western side than the eastern side, particularly in the shallow water south of the Tiwi Islands (Supplemental Figure S1). Likewise, salinity is generally higher on the western side than the eastern side (Supplemental Figure S2). The underway data also show warmer, saltier, denser water to the east and south of the TS5 and TS6 sites (Supplemental Figures S1 and S2). Profiles from additional nearby sites east and west of TS5 and TS6 confirm warmer, saltier, denser water below 10 m east of TS5 and TS6 (red lines in Fig. 9) and cooler, fresher, less dense water west of these sites (blue lines in Fig. 9).

The water is very shallow east of the time series sites and TS5 and TS6 were collected in spots that were slightly deeper than their surroundings. A combination of warming of the water column and evaporation have a stronger effect on the water column in shallower water than deeper water due to less volume of water, and increase the potential temperature and salinity more than in deeper water. This essentially generates warmer, saltier water in shallower regions. The deeper water to the west and north of the Time Series 5 and 6 sites is cooler and fresher.

A trench was a potential offshore water source on the western side (Fig. 1). A short time series, TS8, with ten CTD casts covering a 9 h period was collected at the southern end of this trench. TS8 had cooler,

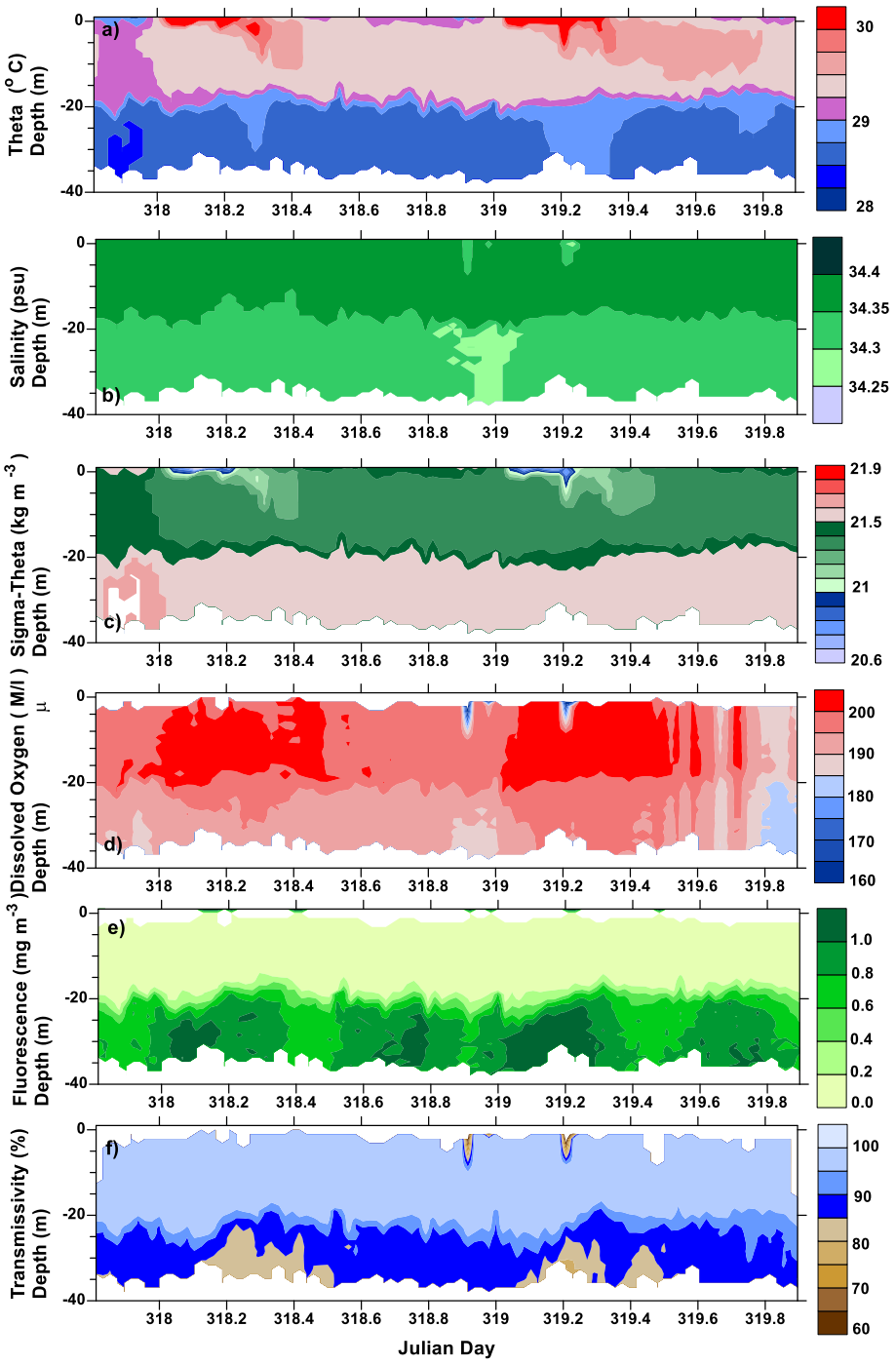

Fig. 3. A) Potential temperature, b) salinity, c) potential density, d) dissolved oxygen, e) fluorescence, and f) transmissivity during Time Series 4 on the east side of the Tiwi Islands.

fresher water (Fig. 9 (black line) and 10) than TS5 and TS6 (Figs. 4 and 5). TS8 was also higher in dissolved oxygen and fluorescence than TS5 and TS6 (Fig. 10d and 10e). TS8 occurred slightly after a neap tide and shifted from a southerly to northerly flow (Fig. 11b). Unfortunately we were unable to collect a complete diurnal or semidiurnal cycle. The water column was stable in the upper 10 m with the strongest stratification between 20 and 30 m (Fig. 10c). The North-South velocities, along the trench, were stronger, but essentially barotropic (Fig. 11b). The East-West velocities, across the trench, were slightly baroclinic in the upper 70–80 m with velocities peaking at 30–40 m (Fig. 11a).

4.2. Forcings

The primary physical forces involved here were tides, solar radiation, winds, and benthic friction, in order of dominance. Other usually relevant processes, such as major geostrophic currents, alongshore coastal currents, or eddies, did not play a significant role. The strong role of tides and the lack of a mean current is evident in the depth averaged tidal ellipses from the SADCP velocities during all three time series (Fig. 12a-c). Although tides are the primary forcing process in the region, the minor roles of solar radiation, winds, and precipitation will be discussed first. Since there is no data on benthic friction, it will not be discussed, although we recognize its key role in mixing, particularly

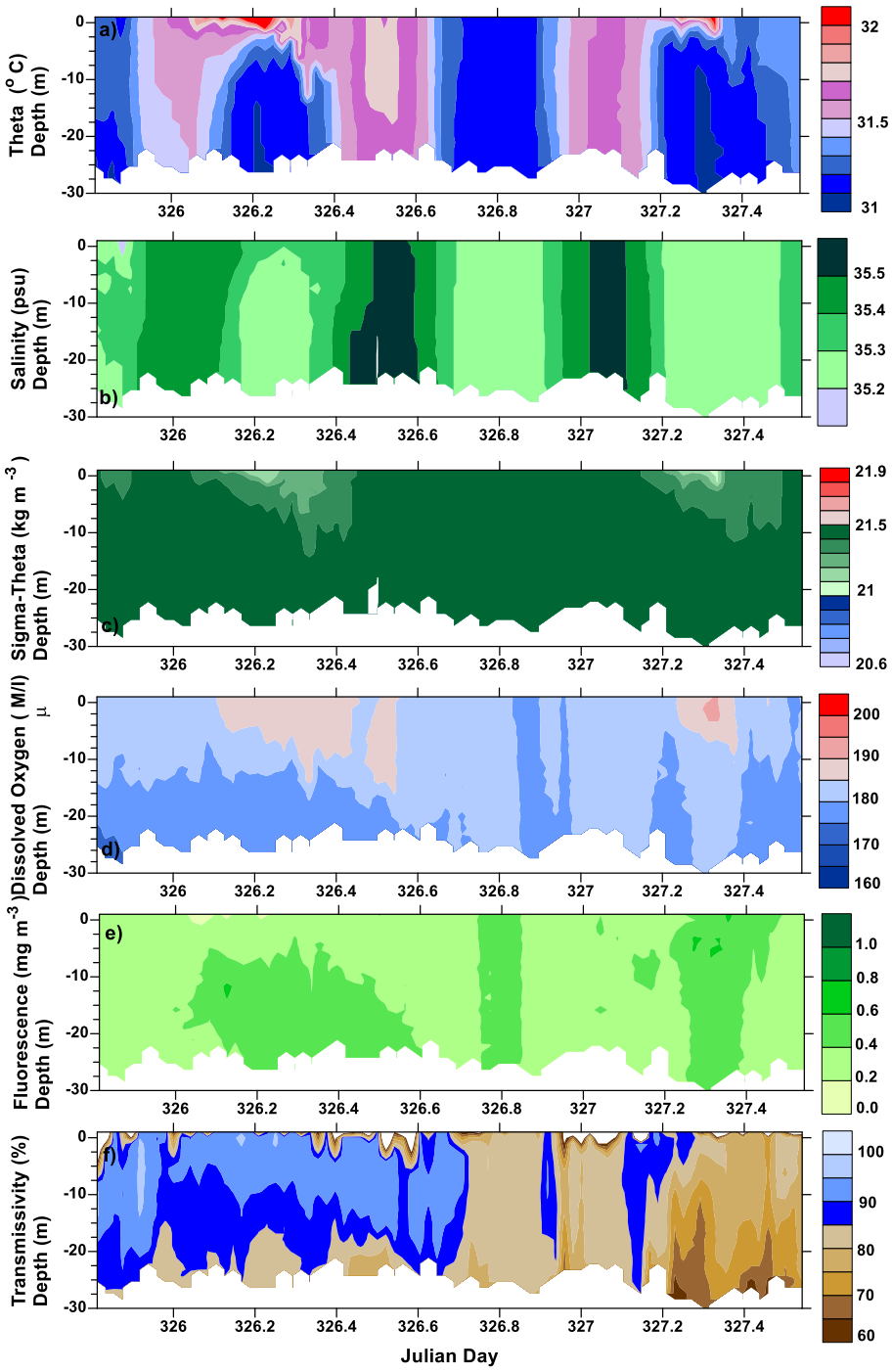

Fig. 4. A) Potential temperature, b) salinity, c) potential density, d) dissolved oxygen, e) fluorescence, and f) transmissivity during Time Series 5 on the west side of the Tiwi Islands.

within the benthic boundary layer.

4.2.1. Solar radiation and precipitation

Solar radiation played a significant role, primarily at the surface. The effects of the incoming solar radiation are shown in Fig. 3b, 3c, and 3df. Solar warming can be seen in the potential temperatures in TS4 starting just before days 318.0 and 319.0 (Fig. 2b and 3a), in TS5 starting days 326.0 and 327.0 (Fig. 2d and 4a), and in TS6 starting day 338.0 (Fig. 2f and 5a). Note that the times are in UTC and this location is UTC + 9:30. The times of sunrise and sunset are about 4:55 and 20:15 local time and 19:25 and 10:45 UTC or 0.81 and 0.44 in decimal day, respectively. The surface warming became noticeable ~ 0.2–0.4 of a day after sunrise. The warming depended on the cloud cover. It was often cloudy in the mornings and was cloudy most of day 337, decreasing the solar warming then. Day 338 was sunny and clear from early morning; consequently, the temperature increase commenced 0.1 of a day earlier and was > 0.4 °C (Fig. 5a), which was stronger than for TS5. Higher temperatures clearly reached depths of 10–15 m (Fig. 3a-5a), which is a combination of the solar warming and vertical mixing. The effect of the warmer water is also clear in the Brunt-Väisälä frequency, N (Fig. 6c, 7c, and 8c for TS4, TS5, and TS6, respectively). N was high at the surface during warming and sank in the water column until it reached the thermocline (~20 m) for TS4 (Fig. 6c) or the bottom for TS5 and TS6 (Fig. 7c and 8c, respectively). Nighttime longwave radiation cooled the surface,

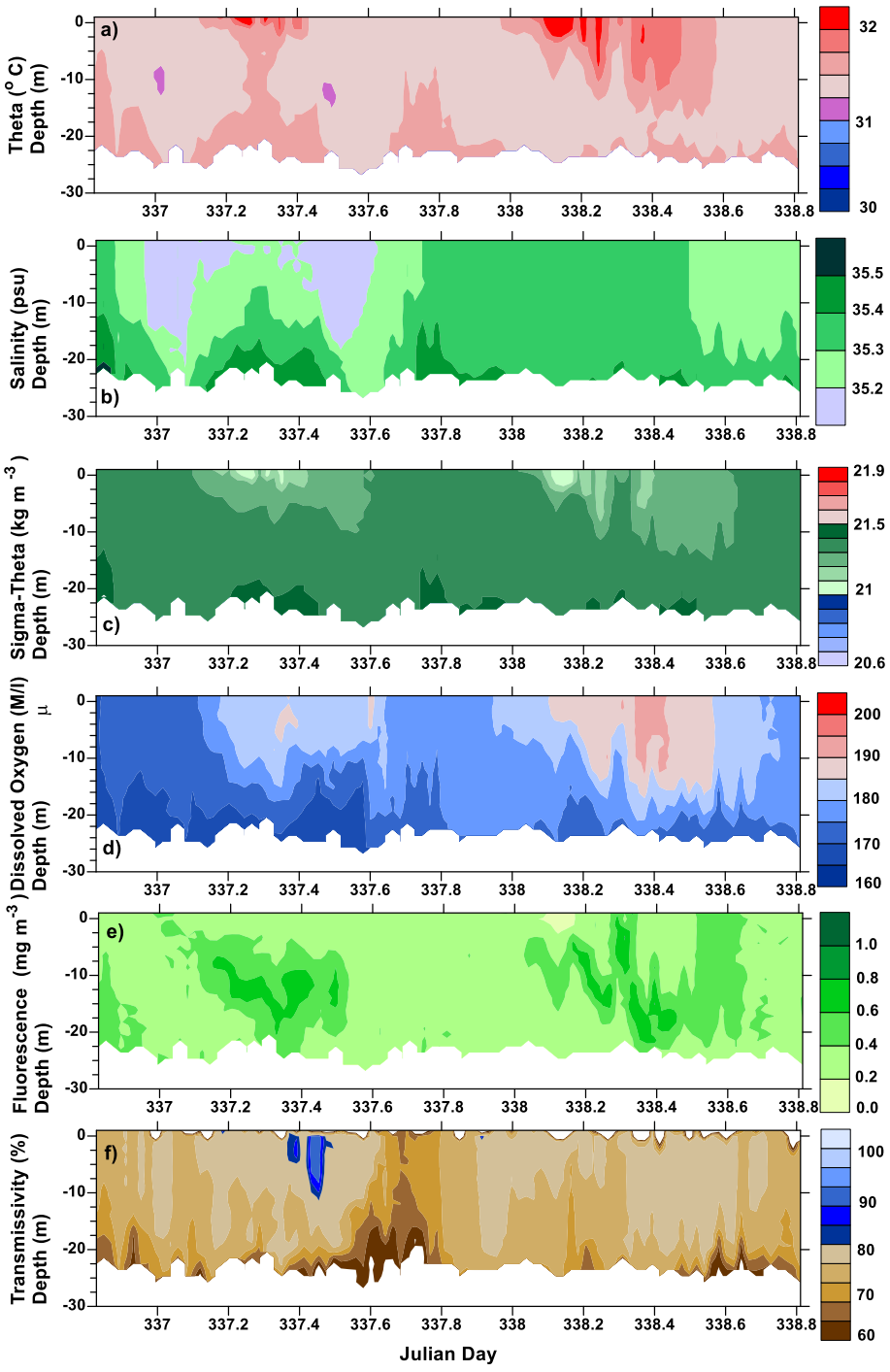

Fig. 5. A) Potential temperature, b) salinity, c) potential density, d) dissolved oxygen, e) fluorescence, and f) transmissivity during Time Series 6 on the west side of the Tiwi Islands.

lowering the surface N from $>$ 15 cph to a background value $<$ 3 cph (Fig. 6c, 7c, and 8c).

Despite having daily thunderstorms, it seldom rained at the ship (Fig. 2a, 2c, and 2e). During TS5, there was one brief rain storm over the ship dropping 7–8 mm of rain, which started a quarter of an hour after the first TS5 cast and ended before the third cast and missed the rain gauge used in Fig. 2. The effect of the storm can be seen as an anomalously low salinity (Fig. 4b) and potential density (Fig. 4c) in the upper 6 m before day 326; however, the lowest salinity occurred 1 h after the storm was at the ship. Since there were other rain storms scattered in the vicinity and runoff from rain storms on land, this salinity minimum is believed to be due to advection of rain water from other location(s) past the ship.

4.2.2. *Winds, Upwelling, and inertial dynamics*

Winds followed a daily sea breeze pattern reaching 8–10 m/s, with the exception of TS5 (Fig. 2). Winds were stronger, 14 m/s from the NW, during the first day of TS5 then reduced to ~ 2 m/s during the second day (Fig. 2c-d) and they were lighter during TS6. The weak winds, primarily on-shore, along with the weak Coriolis force in the tropics were not conducive for strong upwelling. Although inertial oscillations are possible, the time series length (~2 days) is less than their period of ~

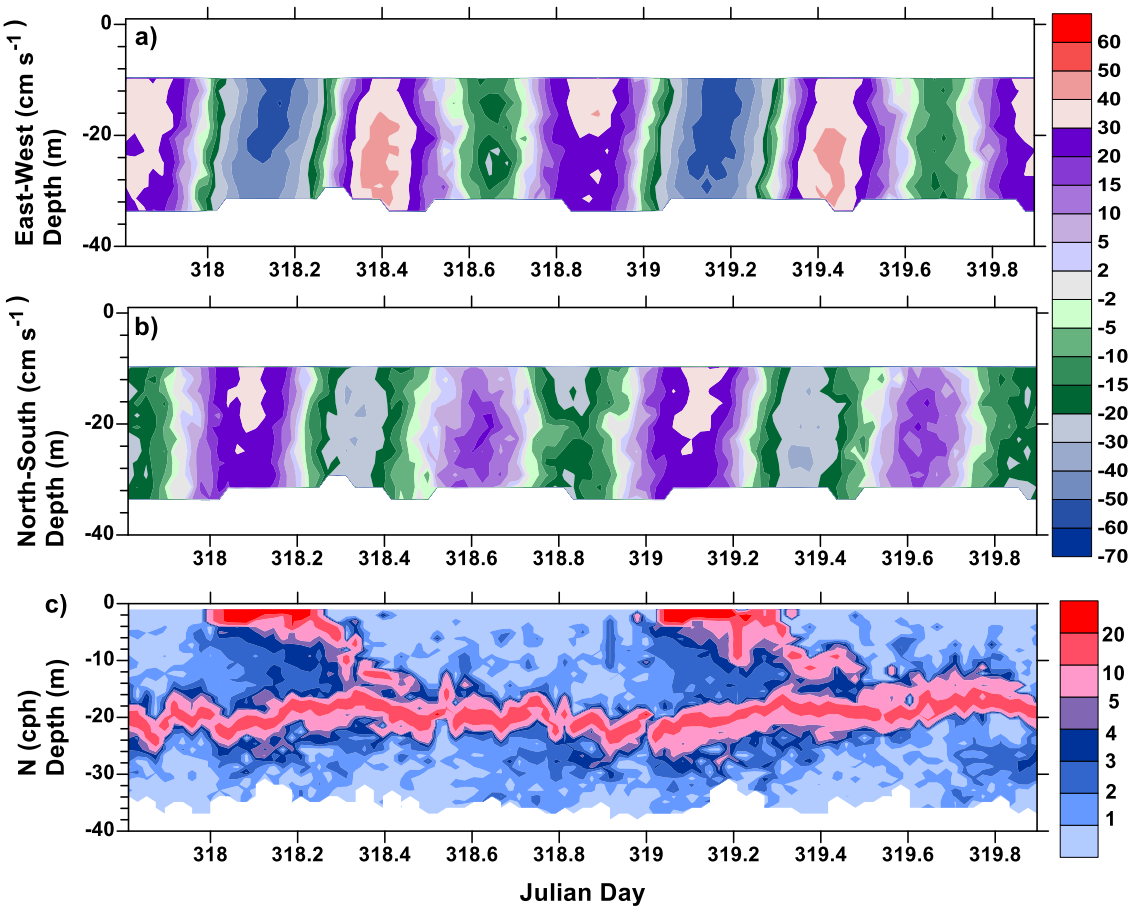

Fig. 6. A) The east-west and b) the north-south velocities during Time Series 4. c) The Brunt-Väisälä frequency during this time.

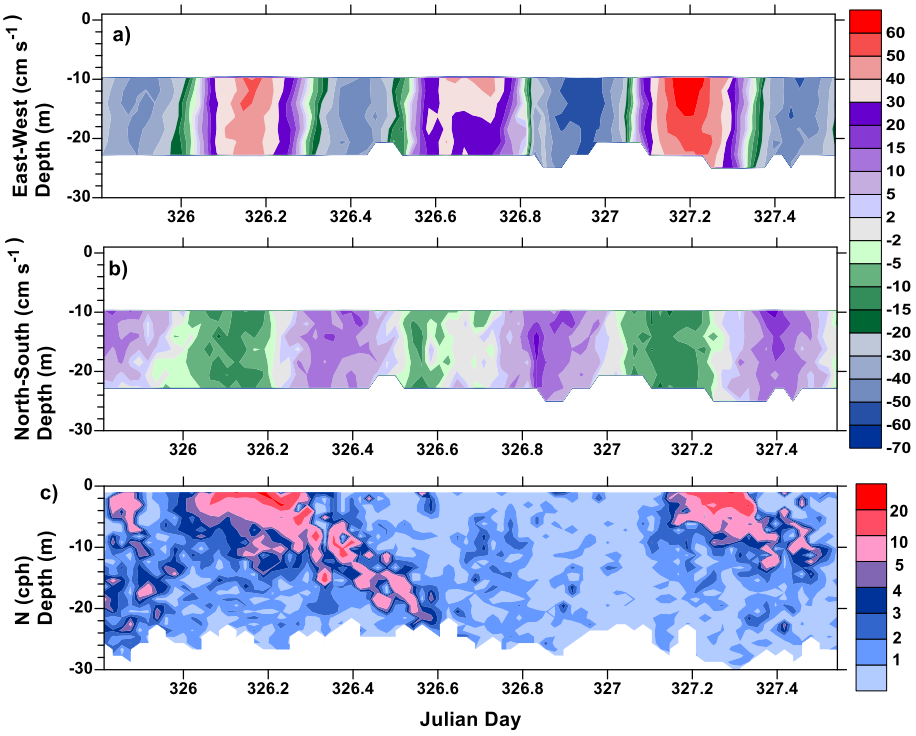

Fig. 7. A) The east-west and b) the north-south velocities during Time Series 5. c) The Brunt-Väisälä frequency during this time.

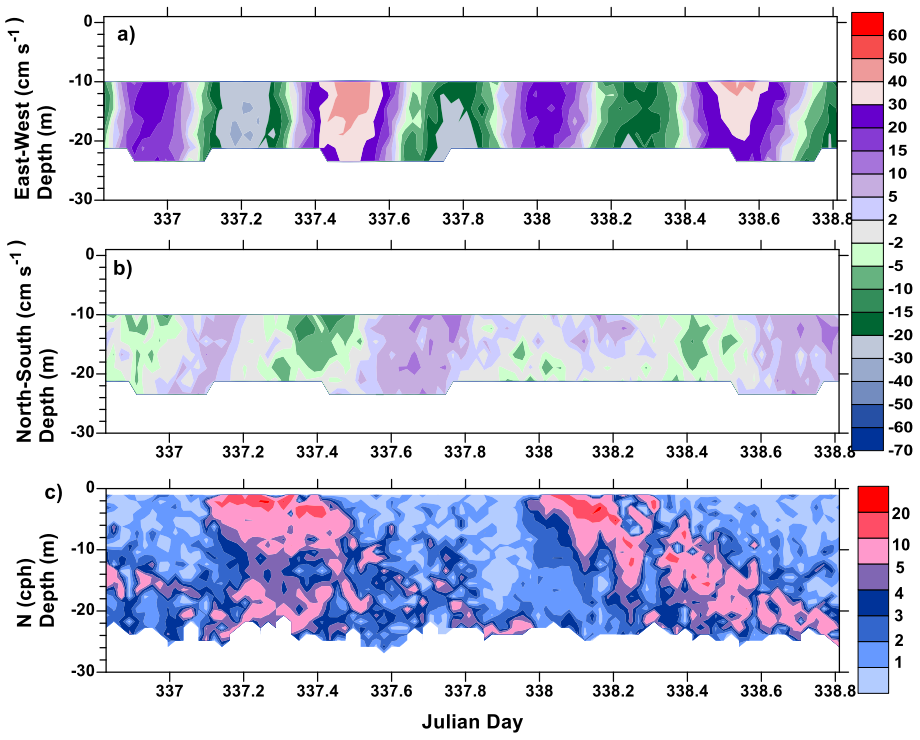

Fig. 8. A) The east-west and b) the north-south velocities during Time Series 6. c) The Brunt-Väisälä frequency during this time.

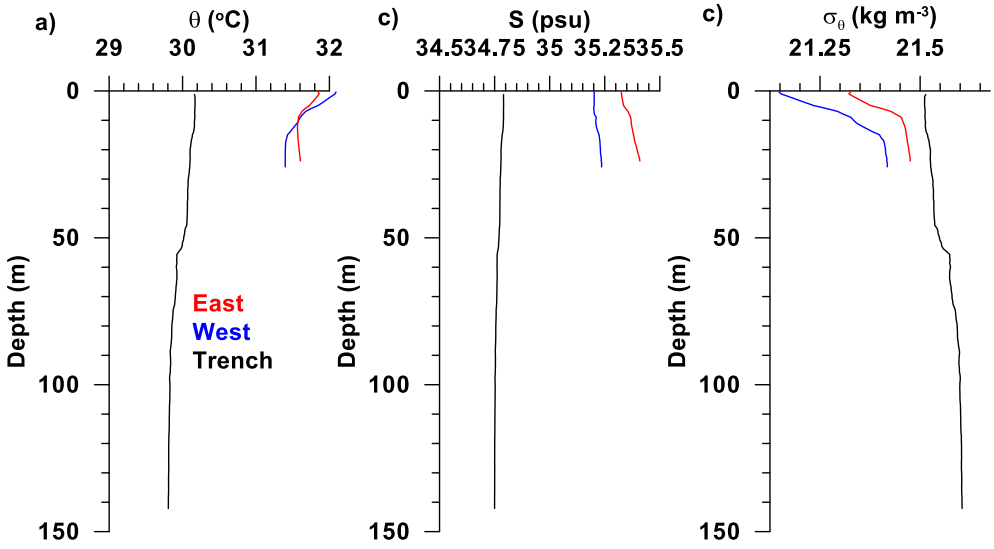

Fig. 9. Profiles of a) potential temperature, b) salinity, and c) potential density against depth from east of Time Series 5 and 6 (red), west of Time Series 5 and 6 (blue), and in a trench west of Tiwi Islands (black).

2.3 days and the SADCP currents do not indicate their presence (Fig. 12).

4.2.3. Barotropic tides

Tides in nearby Darwin are quite large with a range of ~ 8 m (https://www.bom.gov.au/oceanography/projects/ntc/nt_tide_tables.shtml) [Chapman, 1903]. TS4 was collected during a spring tide, TS5 and TS6 near neap tides. Nevertheless, the tidal ranges for TS5 and TS6 of ~ 4 m and ~ 2 m respectively, were nearly equivalent to that for TS4 of ~ 3 m. These tidal ranges were estimated from the maximum pressure converted into depth combined with the CTD altimeter reading.

Tidal currents were slightly stronger on the western side of the Tiwi Islands and Coburg Peninsula than the eastern side with velocity magnitudes of 48 cm/s and 26 cm/s during neap tides on the western side against 44 cm/s during spring tide on the eastern side (Figs. 6-8). Stronger tides in the west agreed with stronger tides on that side in the TPXO8.2 estimates (not shown). Semidiurnal tides dominated on both sides, although a diurnal signal was present along with the semidiurnal signal (spectra not shown). The net mean currents on the west side were much stronger, 3.5–3.9 cm s^{-1}, than for the east side with 1.5 cm s^{-1}; however, for all of them the amplitude much smaller than those of the tidal currents. The barotropic kinetic energies for TS4 and TS5 were similar, 530 J m^{-3} and 653 J m^{-3}, respectively; however, it was much lower for TS6, 201 J m^{-3}, due to weaker velocities, particularly in the North-South direction.

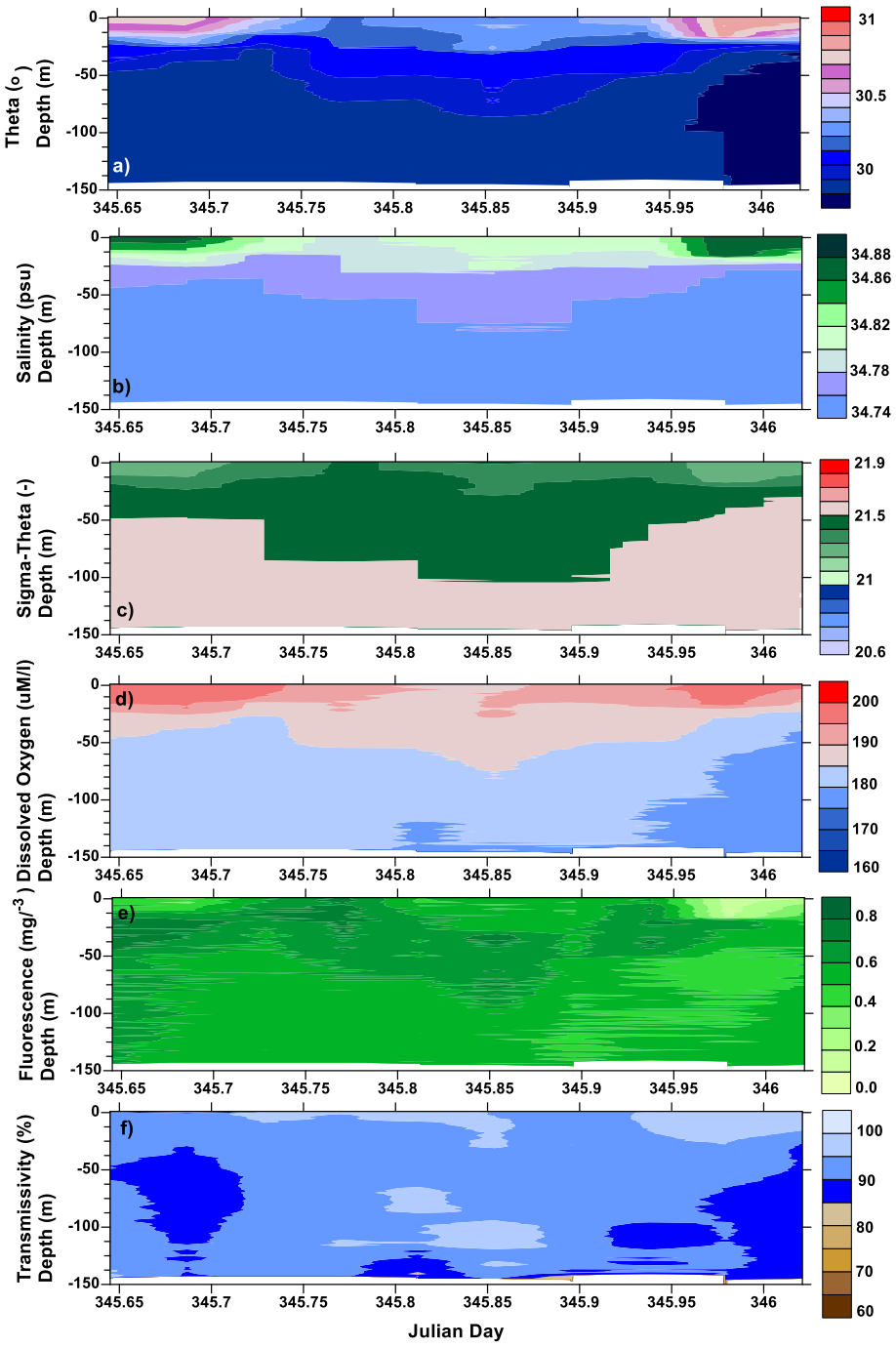

Fig. 10. A) Ootential temperature, b) salinity, c) potential density, d) dissolved oxygen, e) fluorescence, and f) transmissivity during Time Series 8 in the trench on the west side of the Tiwi Islands.

4.2.4. Baroclinic tides

The baroclinic anomalies, u_a and v_a, for both the East-West and North-South horizontal velocities, respectively, were calculated for all three time series. And defined as the difference between the horizontal velocity and the depth-averaged horizontal velocities at a specific location according to.

$u_a(x,y,z,t) = u(x,y,z,t) - U(x,y,t)$ for the East-West direction (1)

$v_a(x,y,z,t) = v(x,y,z,t) - V(x,y,t)$ for the North-South direction (2)

where u and v are the East-West and North-South velocities and U and V are the East-West and North-South depth-averaged horizontal velocities, respectively. Spectra of the baroclinic anomalies for TS4 indicated both semidiurnal and diurnal energy, particularly below the surface (Supplemental Figure S3), although due to the short time series, the spectra have wide confidence intervals. The kinetic energies of the baroclinic anomalies for TS5 and TS6, were weaker, 26 J m^{-3} and 25 J m^{-3}, respectively, than for TS4, 34 J m^{-3}, reflecting the stronger baroclinicity at TS4. The TS4 baroclinic anomaly velocities on the east side were also less chaotic and primarily diurnal, ranging from 5 to 10 cm/s (Fig. 13a,d). Baroclinic anomalies on the west side were smaller for TS5 (Fig. 13b, e) and weaker and more chaotic for TS6 (Fig. 13c, f). The East-West velocity dominated at all sites, with the tidal ellipses ~ 6° off the horizontal. At TS4, the North-South velocity played a larger role with a magnitude of ~ 67% of the East-West velocity; however, it was well correlated, 0.9, with the East-West velocity, lagging by ~ 1.5 h (Supplemental Fig. S4a).

During TS4, the baroclinic anomalies indicated an upward

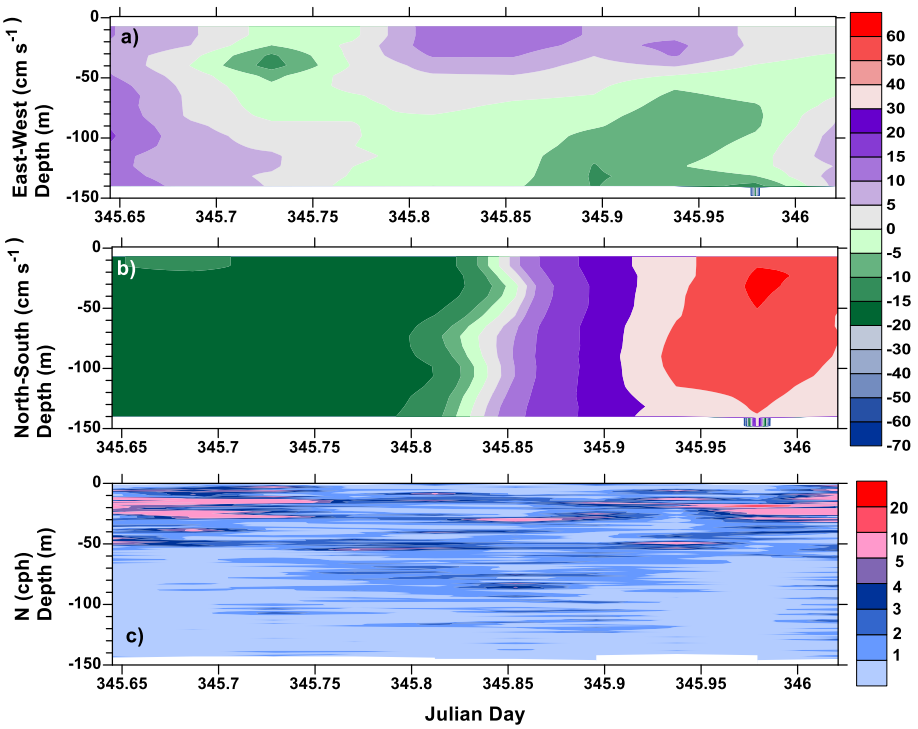

Fig. 11. A) The east-west and b) the north-south velocities during Time Series 8 in the trench on the west side of the Tiwi Islands. c) The brunt-väisälä frequency during this time.

propagating phase of an internal tide (downward propagating energy) at a diurnal frequency and a very slow speed (~8x10^{-4} m s^{-1}) (Fig. 13a,d). Empirical Orthogonal Function (EOF) analysis of the baroclinic anomalies indicated a strong diurnal signal in both the East-West and North-South velocities anomalies of ~ 64% and ~ 44% (Fig. 14a and 14c, respectively). These EOF diurnal signals not only contain the diurnal tides, but also the daily solar and sea breeze cycle signals (Fig. 2). Both of the first two EOFs present were low mode, with the first EOF showing a two-layer internal tide and the second mode intensified velocities at the thermocline and opposite velocities in the upper and lower layers compared to the thermocline (Fig. 14b and 14d for the East-West and North-South velocities, respectively). Higher mode signals comprised ~ 30–40% of the variance, except for the North-South velocities for TS5, where they were ~ 50% of the variance (Supplemental Figures S5-S10).

4.3. Nearby IMOS mooring observations

Some additional insight into the hydrodynamics of the region can be gained from the nearby IMOS moorings. Temperatures from the nearby LYN mooring in 203 m water depth were well-mixed, within 0.5 °C, in the upper 40 m through most of the year (Supplemental Fig. S11a), with the surface warming appearing after day 280. The velocities in the upper 40 m were also essentially uniform with depth and tidal phase (Supplemental Fig. S11b and S11c). This indicates that it is not unusual for the water column to be well-mixed in the upper 40 m in this area. The mean current velocities at the LYN mooring were eastnortheast with a magnitude of ~ 6.3 cm s^{-1} (~6 cm s^{-1} in the east–west direction and ~ 2 cm s^{-1} in the north–south direction). The mooring indicated currents < 10 cm s^{-1} in the upper 30 m during TS4, TS5, and TS6. The background currents alternated between east and west on roughly a 60 day cycle. LYN is north of the time series sites, located in deeper water nearer the continental shelf break. These alternating currents do not appear to be present in our time series. Also LYN experiences stronger currents than those present at the time series locations, particularly at the sheltered locations of TS5 and TS6. The warming of surface temperatures after day 280 reflects the increased daylight hours. The IMOS mooring at Darwin, DAR, is in 12 m of water, and although the Darwin mooring was not operational at the time of the voyage, it does indicate that typically the velocities are strongly tidal and barotropic (Supplemental Figure S12). Unfortunately, there are no IMOS moorings on the east side.

4.4. Dissolved Oxygen, Fluorescence, and Transmissivity

Dissolved oxygen concentrations, fluorescence, and transmissivity also differed between the eastern and western time series. Dissolved oxygen concentrations were much higher on the eastern side (Fig. 3d) than on the western side (Fig. 4d and 5d); however, both increased as the warmer water due to solar radiation reached deeper in the water column, reflecting surface inputs.

Fluorescence on the western side (Fig. 4e and 5e) was high throughout the water column, whereas on the eastern side, high fluorescence was restricted to below the thermocline (Fig. 3e). When integrated over the water column, the fluorescence on the eastern side was roughly twice that on the western side. Transmissivity was high for TS4 and TS5 when the fluorescence was high (Fig. 4e and 5e), with the exception of the first day of TS5, where low transmissivity values in the upper layer, roughly corresponded to the warmer temperatures from solar radiation and high dissolved oxygen (Fig. 4f). This is the time of the strongest sea breeze, ~14 m/s from the Northwest.

4.5. Dynamics

Despite tides being the major forcing processes on both sides of the Tiwi Islands, like the hydrography, the dynamics differed between the two sides. As will be shown, on the western side, strong tidal advection dominated; while on the eastern side, a two-layer diurnal internal tide was present along with tidal advection. The daily solar radiation/nighttime convection cycle, mixing by sea breezes, and, of course, benthic mixing due to friction from the strong tidal currents also contributed significantly.

Since tidal currents dominated, tidal advection can be identified through correlations, if the water properties vary horizontally. Due to

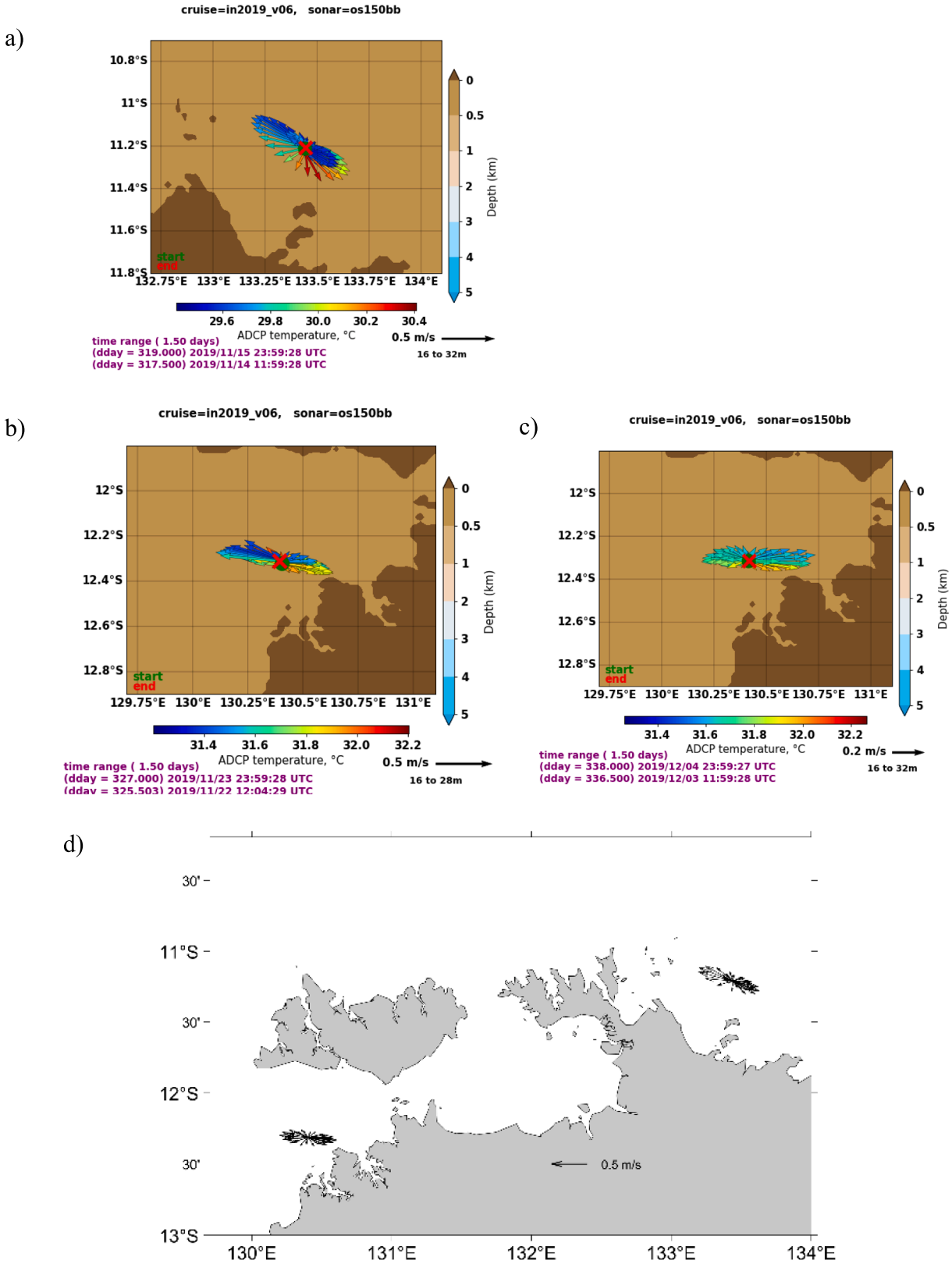

Fig. 12. Current vectors during Time Series a) 4, b) 5, and c) 6 from the shipboard ADCP and d) from the tidal simulation.

warming by the solar cycle affecting temperature, salinity correlations are preferred to identify tidal advection, although correlations for potential temperature were also determined (Supplemental Fig. S4b, S13b, S14b). Looking at correlations for TS4, changes in salinity (Supplemental Fig. S4d) below 20 m lagged changes in the East-West velocity by ~ 3 h with a correlation of ~ 0.8 (positive changes with a southward flow). Changes in the upper water column had the opposite correlation sign (Supplemental Fig. S4d). For TS5, correlations of the

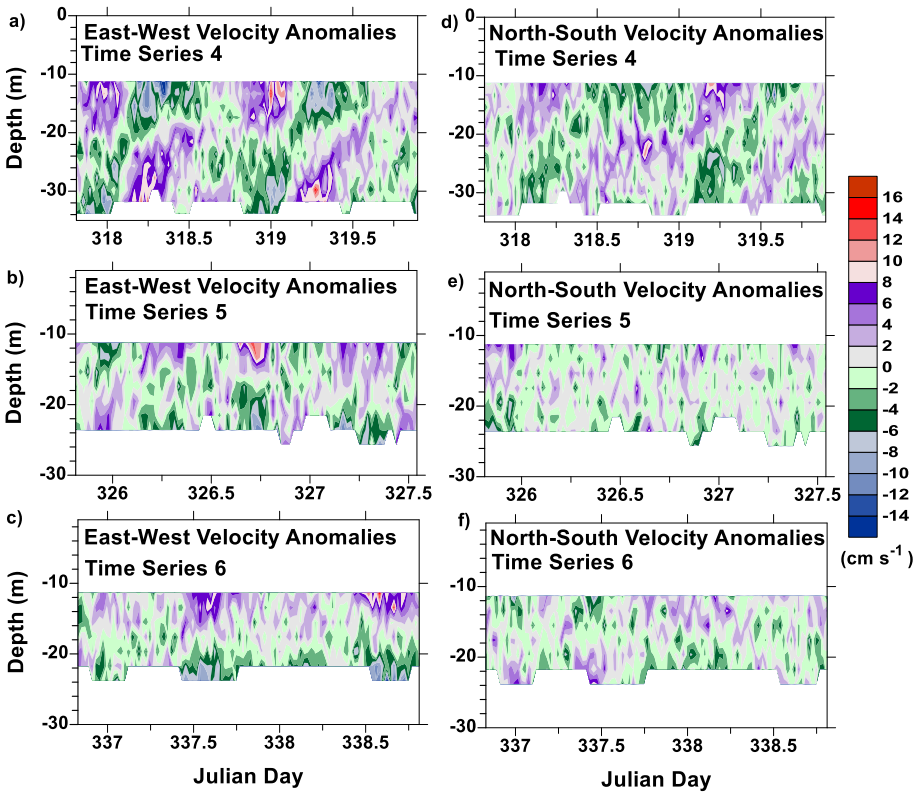

Fig. 13. The baroclinic anomalies in the a) East-West velocities during a) Time Series 4, b) 5, and c) 6 and in the c) North-South velocities during Time Series d) 4, e) 5, and f) 6.

East-West velocity with the salinity (Supplemental Fig. S13b) (~0.8) indicate that the salinity changes ~ 2–3 h after the East-West velocity changes (positive change with a westward flow). The correlations were weaker for TS6 (Supplemental Fig. 9d) and limited to below 20 m depth (~-0.7) with a lag of ~ 2 h (positive change with a westward flow). Currents do not appear to play a role in these low correlation values.

On the eastern side, potential temperature changed in the deeper layer by < 0.2 °C during half of a semidiurnal tidal cycle during TS4 (Fig. 15a), while the salinity changed < 0.05 psu (Fig. 15d). In Fig. 15, the red profiles were taken from a time with maximum eastward flow, the blue ones from a time with a maximum westward flow, and the black ones from slack tide. The profiles from TS5 and TS6 were selected likewise; however, the times were adjusted by 2 h for TS5 and TS6, based on the aforementioned correlations. This lag reflects the time it takes for a different type of water, generated in another location, to pass the time series site. Water with the same characteristics will not show up in the correlations, which are triggered by differences.

Changes in potential temperature and salinity in the lower water column were much larger for TS5 with potential temperature changes of ~ 0.5 °C (Fig. 15b) and > 0.15 psu (Fig. 15e). Salinity changes for TS6 were roughly the same as for TS5 (Fig. 15f); however, the temperature fluctuations were much smaller, less than half as large (Fig. 15c). Focusing on the lower water column to avoid density changes due to the daily solar warming, density changes were greatest during TS6 (Fig. 15i) and equivalent between TS4 and TS5 (Fig. 15g-h, respectively). It is clear in Fig. 15, that temperature plays a bigger role in density changes on the east side (Fig. 15g) and salinity plays a bigger role for TS6 (Fig. 15h-i). This indicates that warmer water was advected from the southeast at TS4 and warmer, saltier water from the east at TS5 and TS6. Depths were shallower southeast and south of TS4 and to the east of TS5 and TS6. Off Australia, shallower water with low runoff is recognized as a generation site of warmer, saltier water due to solar radiation and evaporation.

4.5.1. *Western side dynamics*

Most of the temperature and salinity variations in TS5 and TS6 are believed to be alternating advection of warm, saltier water from the shallower water depths to the east, during a westward flow, and cooler water from the deeper locations to the west during an eastward flow. The increases in salinity outweigh the ones in temperature, generating denser water that sinks as it travels offshore (Fig. 5). Cooler, fresher water (black lines in Fig. 9), such as that in the trench (Fig. 1), replenish the inflow waters. Vertical mixing homogenizes the water column, particularly in this region of shallow water and strong tides, with the tides inducing benthic mixing. Also the warmer waters from the shallow regions are high in dissolved oxygen, turbidity, and fluorescence (not shown). The western side had extensive shallow regions, not only south of the Tiwi Islands, but also further to the west on the other side of the trench (Fig. 1). Since the water column is only weakly stratified at the trench site, it is believed that the water column becomes well mixed from a combination of the daily overturning cycle and benthic tidal friction. The influence of the shallow water on the western side was supported by the tidal modeling study, which showed both a well-mixed water column and the generation of warm, saltier water in the shallow waters around the time series sites, flowing away from shore near the bottom. In addition, the model also indicated a westward flow of the waters formed in the shallow waters east of the Tiwi Islands and Coburg Peninsula. The shallower depths surrounding TS5 and TS6 also prevent the flow of cooler, fresher water from reaching these sites.

4.5.2. *Eastern side dynamics*

On the eastern side, the dynamics were dominated by a two-layer internal tidal system with the transition at 20 m, along with daily solar radiation/nighttime cooling (Fig. 3). As discussed earlier, tidal advection was also present. The upper layer was warmer and saltier than the lower layer. The lower layer was cooler, fresher, more turbid, and higher in fluorescence. The daily solar cycle increased the stratification

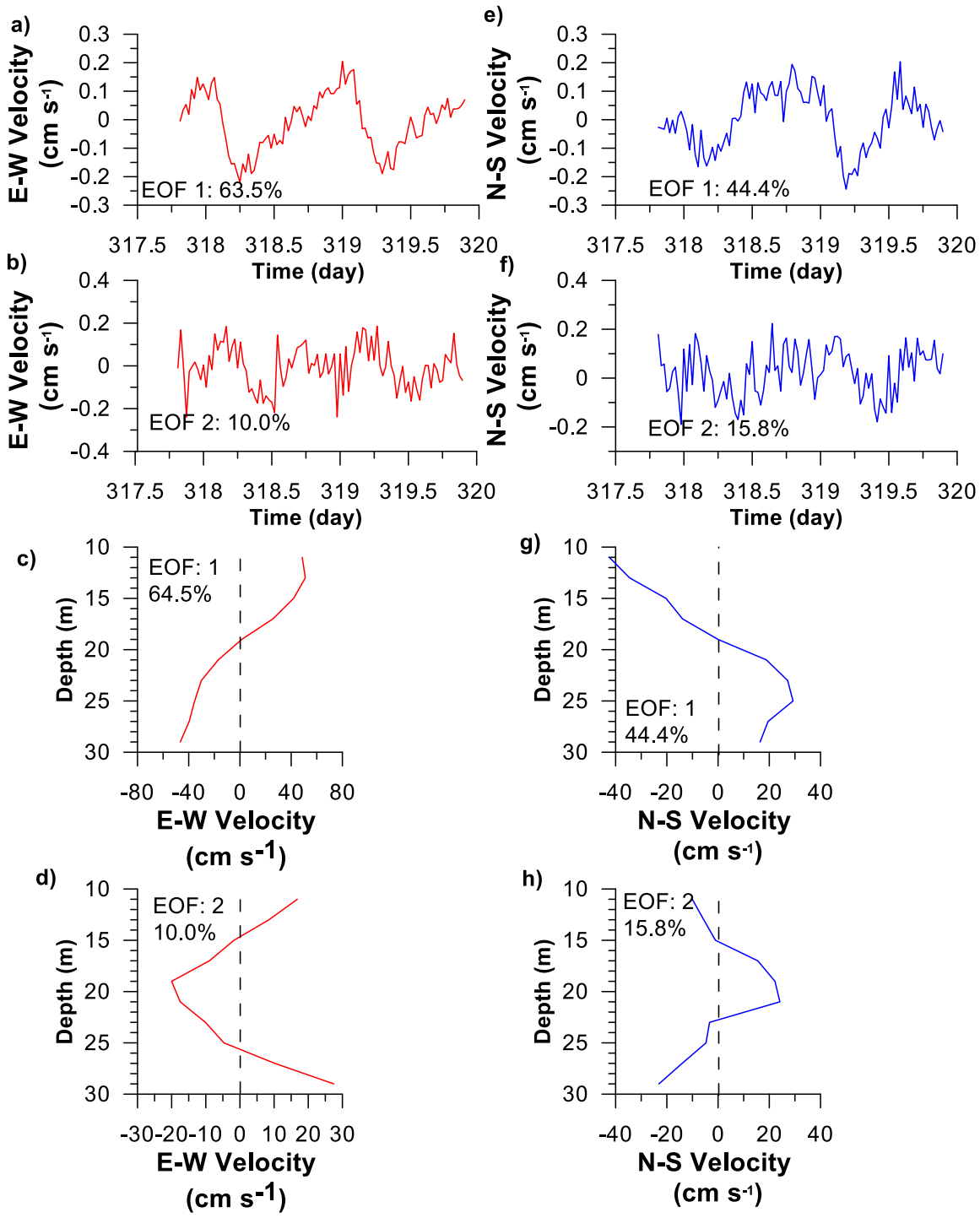

Fig. 14. The first two EOFs for the a–d) East-West (red line) and e–h) North-South (blue line) velocities, during Time Series 4, showing the a, b, e, f) time dependence and c, d, g, h) depth dependence. The eigenvalues are provided as percentages.

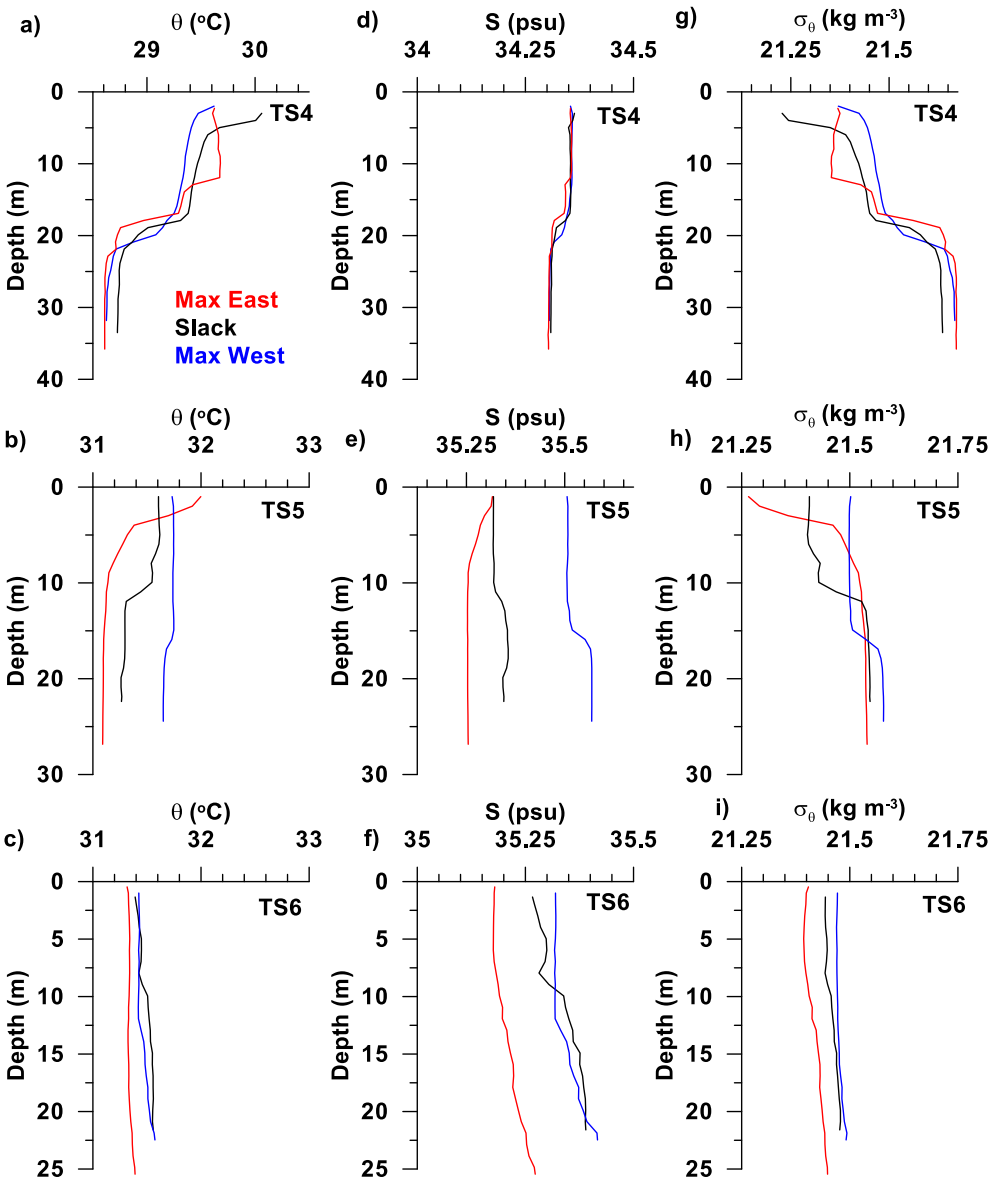

Fig. 15. Profiles of a–c) potential temperature, d–f) salinity, and g–i) potential density during Time Series 4 (a, d, g), 5 (b, e, h) and 6 (c, f, i) from the times of the maximum eastward (red) and westward (blue) velocities and slack tide (black).

in the upper layer and this increase sank in the water column with time to the thermocline, with the surface temperature cooling overnight. In general, the topography was deeper and gently sloping on the eastern side compared to the western side with its extensive, relatively flat, shallow areas.

4.6. *Primary productivity*

Primary productivity as characterized by the fluorescence measurements behaved differently during the different time series; however, it responded to the daily solar cycle for all the time series, increasing just after the surface warming started. It also responded to the tides, similar to previous research, as Cloern (1991) and Sharples (2008), who have found fluorescence to be correlated with the tidal cycles. On the eastern side, TS4, there was a strong 12.4 hr signal and a weaker 6 hr signal in the fluorescence, which coincided with the semidiurnal tide and the entrainment and sinking of particles due to changes in the tidal velocities, respectively (Fig. 3). Since fluorescence was higher only in the lower layer, correlations are only high in the lower layer (Supplemental Fig. S13f-g). The daily lag between the velocities and the fluorescence was depth dependent. On the western side, there was a weak, deeper fluorescence signal for Time Series 5 (Fig. 4) and a stronger signal for Time Series 6, which followed the daily solar cycle with higher fluorescence below the warmer temperatures and higher dissolved oxygen levels of the daily cycle (Fig. 5). There was no evidence of 6 or 12 hr cycles in the fluorescence on the western side. The lags for the fluorescence were weak for TS5 and strongest for the East-West velocity at minus4 hours. The lags were also depth dependent on this side (Supplemental Fig. S13f-g and S14f-g for TS5 and TS6, respectively). So, despite tidal advection on the western side, tidal effects on the fluorescence were weak.

4.7. *Regional simulations*

When using a simulation to provide additional information on the circulation, it is imperative to evaluate how well the simulation replicates the observed conditions. A regional tidal simulation for the locations of TS4 and TS5 had similar hydrographic structure to the observations. The temperatures and salinities for TS4 were reproduced reasonably well (Supplemental Fig. S15a from the circulation

simulation; note the slightly different scales). For TS5, the structure was reproduced, but the water column was too uniform vertically, too cool by ~ 0.75 °C, and too fresh by ~ 0.35 psu (Supplemental Figure S16a). For TS6, the model did not reproduce the temperature or salinity pattern of the observations, but showed a general cooling and freshening trend (Supplemental Figure S17a). South-North potential temperature and salinity transects of the model results on the west side showed a well-mixed water column for the upper 30 m, both initially and at the end of the simulation (Supplemental Figures S18 and S19 for temperature and salinity, respectively). Similar transects on the east side replicated the two layer structure of TS4 with a tidal front developing only at the southern end adjacent to land and more apparent in salinity (Supplemental Figures S20 and S21 for temperature and salinity, respectively). The bottom of the lower layer did warm slightly, ~0.02–0.03 °C, during the simulation, which is attributed to mixing (Supplemental Figure S20).

4.8. Turbulence

Unfortunately, there were no dissipation observations during the CTD time series. The water depth was too shallow to accurately estimate dissipation or diffusivities from the temperature and salinity measurements. However, Thorpe displacements were determined using the standard method of resorting the density profiles and determining the shift [Thorpe, 1977].

Thorpe displacements represent density instabilities leading to overturning, which is a turbulent mixing process. The Thorpe displacements for the three time series indicate overturns reaching to the thermocline on the east side (Fig. 16a) and to 25 and 20 m on the west side for TS5 and TS6, respectively (Fig. 16b and c), during nighttime cooling events.

5. Summary

In the shallow waters of the southern Timor and Arafura seas near the Tiwi Islands and Coburg Peninsula, tides and the daily solar radiation/nighttime cooling cycle dominated the circulation in the form of tidal advection on the western side and both barotropic and baroclinic tides on the eastern side. In these regions, the relevant forcing factors were reduced to tides and the daily solar radiation cycle, along with the daily sea breezes and probably benthic friction. For this reason, this case study provides an excellent opportunity to examine tidal flow and mixing in isolation of strong background currents or eddies. Despite the

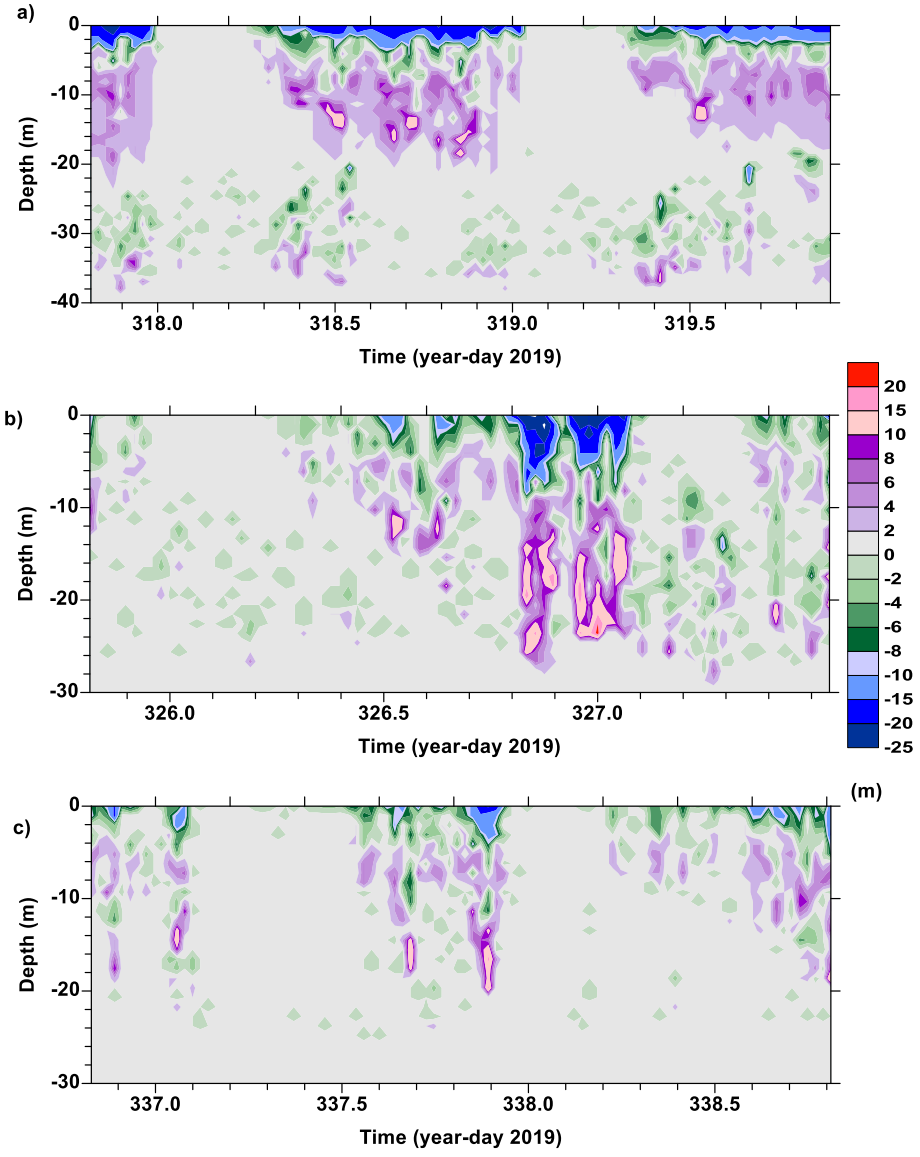

Fig. 16. Thorpe displacements from density during a) TS4, b) TS5, and c) TS6.

prominent forcing being tides and solar radiation with a contribution from mixing by the daily sea breeze, waves, and benthic friction, differences in tidal strength, and variations in the topography resulted in distinctly different dynamical and environmental conditions between the eastern and western sides of the Tiwi Islands and Coburg Peninsula.

On the western side, extensive shallow water (<30 m) regions exist compared to the eastern side, which has a more gently sloping bottom (Supplemental Figure S21). The daily solar radiation cycle on the western side increased the temperature, salinity, and density throughout the water column. The stratification, as represented by the Brunt-Väsälä frequency, increased due to the solar cycle and sank throughout the water column due to mixing, primarily driven by the sea breeze. Cooler, fresher water was present in deeper regions, especially in a trench. However, these waters were denser than the warmer, saltier water and did not flow in near the bottom on the western side or were mixed with warmer water before they reached the study sites, homogenizing the water column. In the shallow water east of the time series sites, evaporation increased the density more than the solar radiation decreased it providing warmer, saltier, denser water. Tidal advection moved this water, encompassing the entire water column, past the time series sites, so alternating warmer, saltier and cooler, fresher water from nearby deeper locations passed the sites. The strong tides also induced mixing due to bottom friction. A combination of surface mixing by the wind, nighttime convection throughout the water column, and benthic frictional mixing homogenized the water column here. The result was the predominance of barotropic conditions on the western side mainly related to tidal advection.

In contrast, the eastern side was baroclinic, with two clear layers separated at ~ 20 m. The density of the lower layer was closer to that in the deeper water offshore as evidenced by a circulation simulation. Although there was a barotropic tide here too, it was slightly weaker than the one on the eastern side and a baroclinic component was present with the two layers moving in opposite directions. Increases in the temperature due to surface radiation affected the upper 20 m more and the stratification increase was limited to this upper layer. The replenishment of colder, fresher water into the lower layer on the eastern side was reflected in an increase in fluorescence. Since fluorescence was limited to the lower water column on the eastern side, while it encompassed the entire water column on the western side, the environment is basically different and there are biological implications, such as the higher primary productivity, for these results.

In summary, the eastern side was dominated by tides, including baroclinic tides, although the daily solar radiation, nighttime convection, and mixing both by the wind and probable benthic friction contributed. More importantly, the solar and atmospheric inputs of heat and freshwater reached throughout the water column on the western side, but were limited to the upper layer above the thermocline on the eastern side.

This baroclinic-barotropic difference in dynamics was due to topographic differences, both blockage by islands or peninsula and/or by differences in bottom characteristics, slope and/or roughness, and could easily occur elsewhere in the world. This would affect biological productivity and penetration of the solar radiation and overturning, as it did in this area. Since water mass production affects the general circulation, there is the possibility that it could influence the general circulation in other regions, although that does not appear to occur here.

The tidal simulation for the east side reproduced the two layer flow and those for the west side the uniform water column. However, those on the west side were too fresh and too cool. The freshness is likely due to less evaporation in the model than in reality. Often models have a minimum depth, which will be deeper than the actual depth, inducing some error but maintaining model stability. Less evaporation and salinity increase will occur in these shallow areas due to their greater depth than actually occurs, causing the water to be fresher. Less warming will occur here in the models, contributing to the lower temperatures in the model simulations. Overmixing by the model also contributes to the differences. The ROMS model has been previously found to overmix the water column especially by wind [Robertson, 2006; Robertson and Hartlipp, 2017; Robertson and Dong, 2019]. The solar radiation budget constitutes the potential cause of the cooling with blackbody radiation exceeding insolation; however, that should affect the entire domain and the cooling occurred mainly on the west side.

The major limitation of this study is the lack of observations. As with most voyages, this interesting case study would benefit by further observations. It would have been nice to have a time series from the eastern side during neap tides. Longer time series would strengthen the results, especially if they could cover an entire spring-neap cycle. This would have to be done at high resolution by either a profiling instrument or mooring, since a CTD time series that long at half hour intervals would likely be interrupted. Keeping any instrument operating for 30 days (28 days is the nominal time for a spring-neap cycle) is a huge challenge, due to both mechanical issues and biological fouling. Measurements in the upper 10 m and within the benthic boundary layer would also add insight, particularly the latter for benthic mixing. Special instruments are needed to obtain that information. Transects on the different sides of the time series sites would provide information needed to further evaluate the dynamics. However, funding for such extensive observations is extremely difficult to obtain. Until then, these are one of the very few observations for this area, which adds to their uniqueness and importance.

Feynman said that turbulence is the most important unsolved problems in classical physics [Eames et al., 2011]. This is still true today and the handling of mixing generated by turbulence is presently recognized as one of the major shortcomings of ocean circulation and climate models [Eames et al., 2011]. The major issue is that a wide range of mechanisms cause mixing and they have a wide range of scales from cm to km. Furthermore, although wind and tides, including internal tides, are widely recognized as the primary turbulence/mixing mechanisms in the ocean, their roles and strengths vary with latitude, location with respect to other currents, depth, time, topography, water depth, hydrography, and other factors. Since many mixing mechanisms are unresolvable at the present resolution for global circulation and climate models, mixing is parameterized in them. Several vertical mixing parameterizations exist and some will perform better in certain situations than others. Knowing which one to use is key to "getting the mixing right". To improve mixing in the ocean circulation models, a large suite of observational-model comparisons covering a wide range of forcing factors and environmental conditions for mixing are needed. This study contributes to that suite of observations available for comparison, with the unique aspect that its main forces are tides and the diurnal cycle, which is a much simpler situation than is present in most of the world's oceans. One study alone is insufficient to evaluate the performance of the parameterization(s) to be used widely, but it does make a contribution to the whole set of observations available for researchers to utilize. And an observational data set with a limited number of forces involved is extremely rare in the ocean.

Author Contributions

R. Robertson was involved in writing the proposal for ship time, planning the observational voyage, participating in the voyage as a co-PI, collecting data on the voyage, analysing the observations, setting up the model simulations, and writing and revising the paper. C. Zhao ran the regional tidal simulations. Z. Xu advised C. Zhao on the model simulations and assisted in writing the paper. Z. Liu assisted in writing the paper and his team was involved in the observational effort. P. S. Hartlipp was involved in the preliminary model set up and simulations before the observational program and participated in collecting and analysing the observations.

Funding

Funding for research was provided by several sources. First, the National Key Research and Development Program of China, 2017YFA0604102. Additionally, an Internal Grant from Xiamen University Malaysia Research Fund XMUMRF/2018-C2/ICAM/0003 "Ocean Mixing in Various Conditions and its Handling in the Regional Ocean Modeling System (ROMS) Model" and grants from "Strategic Priority Research Program" of the Chinese Academy of Sciences No. XDB42000000 and the National Natural Science Foundation of China, 91,858,201 & 92,058,202 & 41721005. The funding for ship time was provided by MNF Grant IN2019_v06 "Maritime Continent observations of atmospheric convection, biogenic emissions, ocean vertical mixing, and the Indonesian Throughflow".

Declaration of Competing Interest

The authors declare that they have no known competing financial interests or personal relationships that could have appeared to influence the work reported in this paper.

Data availability

Data will be made available on request.

Acknowledgments

We would like to thank Australia's Marine National Facility (MNF) and the crew of the RV Investigator for their assistance during this voyage. We would also like to thank our CTD operators and sampling team: Cristina Cerano Guerra, Rob Ryan, Cisco Navidad, Matthias Retsch, and Haydn Trounce. In so many ways, they and the RV Investigator crew made this data set possible.

Data Availability Statement

All the data from the voyage is available from the Australia Open Data Network (AODN) (https://portal.aodn.org.au/; http://thredds.aodn.org.au/thredds/catalog/IMOS/SOOP/SOOP-ASF/VLMJ_Investigator/meteorological_sst_observations/2019/ISAR-QC/catalog.html;). The easiest way to access the voyage data is through the CSIRO Data Trawler (https://www.marine.csiro.au/data/trawler/survey_details.cfm?survey = IN2019_V06). The model simulation output are available upon request.

Appendix A. Supplementary material

Supplementary data to this article can be found online at https://doi.org/10.1016/j.pocean.2023.103057.

References

Blauw, A.M., Nenica, E., Laane, R.E.P.M., Greenwood, N., Huisman, J., 2012. Dancing with the tides: Fluctuations of coastal phytoplankton orchestrated by different oscillatory modes of the tidal cycle. PLOS One 7 (11), e49319.

Chapman, R.W., 1903. Tides at Port Darwin. Nature 68, 295.

Cloern, J.E., 1991. Tidal stirring and phytoplankton boom dynamics in an estuary. J. Mar. Res 49, 203–221. https://doi.org/10.1357/002224091784968611.

Condie, S.A., 2011. Modeling seasonal circulation, upwelling and tidal mixing in the Timor and Timor Seas. Cont. Shelf Res. 31, 1427–1436. https://doi.org/10.1016/j.csr.2011.06.005.

Eames, I., Flor, J.B., 2011. *New developments in understanding interfacial processes in turbulent flows*", *Phil. Trans. of the Roy*. Soc, A. 369, 702–770. https://doi.org/10.1098/rsta.2010.033.

Easton, A. K. 1970. The tides of the continent of Australian, Horace Lamb Centre for Oceanographic Research, Flinders Univ. of South Australia, *Research Paper No. 37*, 1970.

Egbert, G.D., Erofeeva, S., 2002. Efficient inverse modeling of barotropic ocean tides. J. Atmos. Oceanic. Tech. 19, 22475–22502. https://doi.org/10.1029/2003GL019003.

Energy, T., 2019. Clarence Strait Tidal Energy Project. Tethys. http://www.tenaxenergy.com.au/projects.html.

Kampf, J. 2016. On the majestic seasonal upwelling system of the Timor Sea*, J. of Geophys. Res*., 121, 12-18-1228, doi:10.1002/2015JC011197.

Locarnini, R. A., A. V. Mishonov, J. I. Antonov, T. P. Boyer, H. E. Garcia, O. K. Baranova, M. M. Zweng, C. R. Paver, J. R. Reagan, D. R. Johnson, M. Hamilton, and D. Seidov 2013. World Ocean Atlas 2013, Volume 1: Temperature. S. Levitus, Ed., A. Mishonov Technical Ed.; *NOAA Atlas NESDIS 73*, 40 pp.

Moore, L.R., Huang, T., Ostrowski, M., Mazard, S., Kumar, S.S., Gamage, H.K.A.H., Brown, M.V., Messer, L.F., Seymour, J.R., Paulsen, I.T., 2019. Unicellular cyanobacteria are important components of phytoplankton communities in Australia's northern oceanic ecosystems. Front. Microbiol. 9, 3356. https://doi.org/10.3389/fmicb.2018.03356.

Robertson, R., 2006. Modeling Internal Tides over Fieberling Guyot: Resolution Parameterization, Performance. Ocean Dynam. https://doi.org/10.1007/s10236-006-0062-5.

Robertson, R., Dong, C.M., 2019. An evaluation of the performance of vertical mixing parameterizations for tidal mixing in the Regional Ocean Modeling System (ROMS). Geosci. Lett. 6 (15) https://doi.org/10.1186/s40562-019-0146-y.

Robertson, R., Hartlipp, P., 2017. Surface wind mixing in the Regional Ocean Modeling System (ROMS). Geosci. Lett. 4 (24) https://doi.org/10.1186/s40562-017-0090-7.

Schiller, A.M., 2011. Ocean circulation on the North Australian Shelf. Cont. Shelf Res. 31, 1082–2095. https://doi.org/10.1016/j.csr.2011.03.013.

Sharples, J.M., Tweedle, J.F., Green, M., Palmer, M.R., Kim, Y.-N., Hickman, A., Holligan, P.M., Moore, C.M., Rippeth, T., Simpson, J.H., 2007. Spring-neap modulation of internal tidal mixing and vertical nitrate fluxes at a shelf edge in summer. Limnol and Ocean 52 (5), 1725–1747. https://doi.org/10.2307/4502331.

Shchepetkin, A., and J. C. McWilliams 2004. The regional oceanic modeling system (ROMS): a split-explicit, free-surface, topographic-following-coordinate oceanic model, *Ocean Modelling*, 9347-9404, doi:10/1016/j.ocemod.2004.08.002.

Stevens, C.L., Sutton, P.J.H., Law, C.S., 2012. Internal waves downstream of Norfolk Ridge, western Pacific and their biophysical implications. Limno. Oceanogr. 57, 897–911. https://doi.org/10.4319/lo.2012.57.4.0897.

Thorpe, S.A., 1977. Turbulence and mixing in a Scottish loch. Philos. Trans. Roy. Soc. London 286A, 125–181.

Thurnherr, A.M., 2010. A practical assessment of uncertainties in full-depth velocity profiles obtained with Teledye/RDI Workhorse AcousticDoppler Current Profilers. J. Atmos. Oceanic Technol. 27, 1215–1227.

Whiteway, T.,G. 2009. Applying Geoscience to Australia's most important challenges, Record. 2009/21. *Australian Bathymetry and Topography Grid*.